Part 2

Modelling glaciers and ice sheets

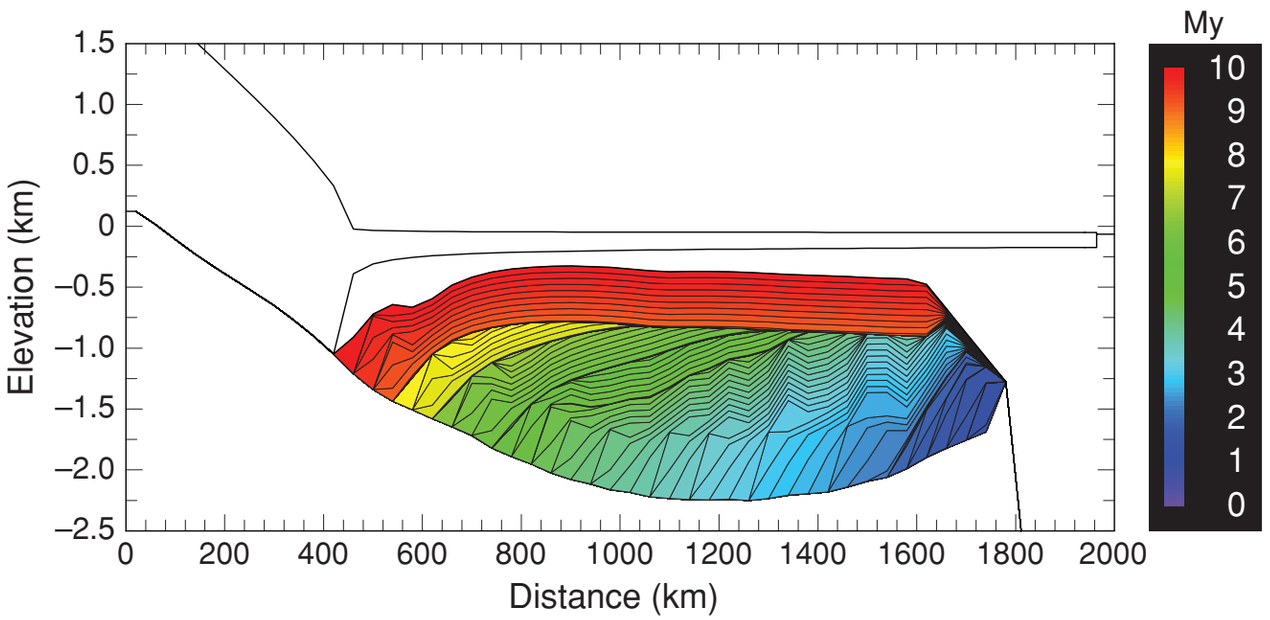

Numerical model demonstrating debris transport on an ice-sheet scale. (Image by D. Pollard and R. DeConto; see following paper)

A coupled ice-sheet/ice-shelf/sediment model applied to a marine-margin flowline: forced and unforced variations

DAVID POLLARD† *and* ROBERT M. DECONTO*

†Earth System Science Center, Pennsylvania State University, University Park, PA 16802, USA (e-mail: pollard@essc.psu.edu)
**Department of Geosciences, University of Massachusetts, Amherst, MA 01003, USA*

ABSTRACT

A standard large-scale ice-sheet model is extended by (i) adding ice stream-shelf flow using a combined set of scaled equations for sheet and shelf flow, and (ii) coupling with a deforming sediment model that predicts bulk sediment thickness. The combination of sheet and shelf flow equations is heuristic, but allows horizontal shear and longitudinal stretching without *a priori* assumptions about the flow regime, and a freely migrating grounding line. The sediment model includes bulk transport under ice assuming a weakly non-linear till rheology, and generation of till by glacial erosion. The combined model explicitly simulates off-shore sediment strata, taking one step towards the goal of direct comparisons with Cenozoic glacimarine sediments on Antarctic continental shelves.

Preliminary 1-D flowline simulations are described on a linearly sloping domain, with simple prescribed spatial and temporal variations of surface ice mass balance. Each simulation is run for 10 million years, and the various patterns of offshore sediment strata built up over the course of each run are examined. A wide variety of sediment patterns is produced depending on uncertain model parameters, including unforced irregular oscillations in the absence of external forcing variations. The results are not conclusive, but illustrate the variety of possible interactions that may play a role as more definitive 3-D models become available to link Cenozoic climate variations with the Antarctic sediment record.

Keywords Ice sheet model, ice shelf model, marine sediment, Cenozoic, Antarctica.

INTRODUCTION

A broad picture of long-term climate variations during the Cenozoic has emerged from deep sea core records (Zachos *et al.*, 2001). Overall cooling since the warm and largely ice-free early Eocene (~50 Ma) has been punctuated by major Antarctic ice growth around the Eocene-Oligocene boundary (34 Ma) and significant fluctuations through the Oligocene and Miocene. These were followed by relatively recent Northern Hemispheric glaciation in the Pliocene, leading to the current Quaternary ice ages. Beyond this broad picture, some important questions remain concerning the role of ice sheets and CO_2 forcing (Pekar and DeConto, 2006; Pekar *et al.*, 2006). Numerous large fluctuations in $\delta^{18}O$ records, especially during the Miocene, suggest ice volume variations of roughly 30 to ~75 m equivalent sea level over time scales of several 10^5 to 10^6 years. On the face of it, that would require drastic retreats and re-growth of the East Antarctic Ice Sheet (EAIS, currently ~65 m sea-level equivalent), and/or similar amounts of Northern Hemispheric ice growth and decay for which there is scant terrestrial evidence. It is important to understand how much these $\delta^{18}O$ fluctuations are due to other factors in the composite record, or whether they imply drastic variations of EAIS since the Oligocene (Oerlemans, 2004a, 2004b; Pekar and DeConto, 2006; Pekar *et al.*, 2006).

Once a large continental-scale EAIS is formed, it is problematic to invoke drastic retreats at least of the terrestrial portions (grounded on bedrock above sea level after rebound), due to hysteresis in

the ice-climate system stemming from ice-albedo and height-mass-balance feedbacks (Huybrechts, 1993, 1994; Maqueda *et al.*, 1998; Oerlemans, 2002). Air temperatures must rise on the order of 15°C around the Antarctic terrestrial flanks before substantial melting and retreat occurs. Depending on model physics (orbital forcing or not, ice-albedo feedback or not), that corresponds to a several fold increase above present atmospheric CO_2, which is not observed in Cenozoic proxy records since the late Oligocene (Pagani *et al.*, 2005). However, it is more plausible to invoke retreats and advances of *marine* portions of Antarctic ice, for instance in Wilkes Land (Miller and Mabin, 1998) or the West Antarctic Ice Sheet itself (WAIS, Anderson and Shipp, 2001; which may have existed since the Miocene at least, Scherer, 1991). Whether or not these have occurred and how much sea level they could account for (~6 m, current WAIS) is an open question.

There is a potential wealth of information on WAIS and EAIS variations in Cenozoic marine sediment deposits on the Antarctic continental shelf (Cooper *et al.*, 1993; Hambrey and Barrett, 1993; Brancolini *et al.*, 1995; De Santis *et al.*, 1999, Anderson, 1999; Escutia *et al.*, 2005; and others). Since the mid-Miocene at least, much of these sediments have been deposited in glacimarine or sub-ice environments, as the ice sheet grounding line has advanced and receded over the continental shelf, especially in the Ross and Weddell Seas, Prydz Bay, and off Wilkes Land and the Antarctic Peninsula. Great efforts have been made over the last several decades to study these deposits by seismic profiling, coring and sampling, and progress in inferring Cenozoic ice-sheet variations is ongoing (Anderson, 1999).

If climate and ice-sheet models can include these sediment processes explicitly and results compared directly with observed deposits, that would be a valuable tool in linking the Antarctic marine sediment record to Cenozoic ice and climate history. As a small step towards that goal, this paper extends a standard ice-sheet model to include (i) both grounded ice-sheet and floating ice-shelf flow, and (ii) sub-ice sediment production and transport, both of which are necessary to explicitly simulate shelf deposits. Preliminary results are described for experiments run over 10 million years with basic 1-D flowline geometries and simple prescribed climate forcing.

COMBINED ICE SHEET-SHELF MODEL

The combination of ice sheet and shelf flow in one efficient large-scale model is not straightforward (Vieli and Payne, 2005). Although grounded (terrestrial) ice and floating (shelf) ice have the same fundamental ice rheology, the large-scale flow regimes and scaled equations are very different. Due to basal shear stress, terrestrial ice flows mainly by vertical shear $\partial u/\partial z$ determined locally by the driving stress $\rho g H \partial h/\partial x$ (the zero-order shallow-ice approximation), whereas shelf ice deforms mainly by along-flow longitudinal stretching $\partial u/\partial x$ determined non-locally by the shelf thickness distribution. In the vicinity of the grounding line and in ice streams with very little basal stress, a combination of the two flow regimes exists. Full(er)-stress equations are available (Blatter, 1995; Pattyn, 2002; Payne *et al.*, 2004) but are computationally expensive, and have only recently begun to be applied in 3-D (Pattyn, 2003). Other approaches have been (i) to add basal and side friction to the scaled shelf equations (MacAyeal, 1989; Dupont and Alley, 2005; Vieli and Payne, 2005), (ii) to use continuum mixtures within each grid cell (Marshall and Clarke, 1997), and (iii) to apply sets of scaled equations (sheet/stream/shelf) in pre-determined domains, with simple matching conditions at the interfaces (Huybrechts, 1990, 2002; Hulbe and MacAyeal, 1999; Ritz *et al.*, 2001; Vieli and Payne, 2005).

The approach used here is to heuristically combine the scaled sheet and shelf equations, and is close to those used by Hubbard (1999, 2006) and Marshall *et al.* (2005). In these techniques, the two sets of scaled equations (for internal shear $\partial u/\partial z$ and for vertical-mean longitudinal stretching $\partial u/\partial x$) are combined into one set, which is applied at all locations with no *a priori* assumptions about flow regimes. Related non-rigorous sets of combined equations have also been used by Alley and Whillans (1984) and van der Veen (1985). The main difference in our approach is that the full elliptical (non-local) stretching equation is retained, which is needed for domains that include floating ice with vanishing basal stress.

The flow equations are described fully in Appendix A (page 48). A numerical iteration is performed at each timestep between the shear and stretching components that converges naturally to the appropriate scaling or to a combination of the

two, depending on the magnitude of the basal drag coefficient. The combination is heuristic because neither set of equations is accurate in the transition region where both $\partial u/\partial x$ and $\partial u/\partial z$ are significant. Nevertheless, our results are reasonable in idealized tests and in 3-D modern Antarctic simulations. Work is in progress to compare them with full-stress solutions in simple flowline situations such as Huybrechts (1998). Our equations fall into type L1L2 of Hindmarsh's (2004) categorization of various approximate schemes, which is found to yield relatively accurate results. Using a similar technique to ours, Hubbard (2000) found that results for a valley glacier agree well with those using a higher-order model.

Hindmarsh (1993, 1996) and Hindmarsh and Le Meur (2001) have investigated whether the dynamics of the narrow transitional region near the grounding line matter for overall equilibrium and stability properties, but these issues remain unresolved. The general behaviour anticipated by Weertman (1974) (cf., van der Veen 1985; Huybrechts, 1998), is that the grounding line can advance relatively freely into water depths of less than a few hundred metres, but advance is inhibited and retreat can easily be induced by greater grounding-line depths; this behaviour occurs in our model with the aid of MacAyeal-Payne thermal fluctuations (Hindmarsh and Le Meur, 2001), and is important in interpreting the results described below. Recently Vieli and Payne (2005) have examined grounding-line migration in 1-D flowline sheet/stream/shelf models using fixed versus moving grids, and found suspect behaviour and grid dependencies with fixed grids. Our grid is fixed, but unlike theirs our equations combine sheet and shelf flow continuously across the grounding line. These issues will be addressed in a separate paper, but we note that the results shown here do not depend strongly on grid size (nominally 40 km), and very similar results are obtained for grid resolutions of 20, 40 and 80 km (not shown).

In addition to the ice flow equations, the ice model consists of three other standard components: (i) an ice-mass advection equation predicting ice thickness and accounting for prescribed annual surface accumulation minus ablation, (ii) an ice temperature equation including ice advection, vertical diffusion in the ice-sediment-bedrock column, and shear heating, and (iii) a bedrock elevation equation with local relaxation towards isostatic equilibrium and elastic lithospheric deformation (Huybrechts, 1990, 2002; Ritz *et al.*, 1997, 2001).

SEDIMENT MODEL

The large-scale, long-term evolution of sediment is simulated using a predictive model of sediment thickness, including subglacial deformation by the imposed basal ice shear stress, which deforms and transports the upper few 10's of cm to meters of sediment. The sediment rheology is assumed to be weakly non-linear (Boulton and Hindmarsh, 1987; Alley, 1989; Boulton, 1996; Jenson *et al.*, 1996), in contrast to nearly plastic (Tulaczyk *et al.*, 2000; Kamb, 2001). The induced sediment velocity contributes to ice motion and effectively makes the bed much slipperier.

The deforming sediment model and equations are described in Appendix B. The main change from our previous applications (Clark and Pollard, 1998; Pollard and DeConto, 2003) is a simple parameterization of fractional exposed bedrock when the grid-mean sediment thickness is <0.5 m. This accounts for separate basal shear stresses over the sediment and bare-bedrock fractions, and assumes that the sediment patches always remain thick enough so sediment deformation never penetrates to bedrock. Where no (or little) sediment exists, quarrying or abrasion by ice on exposed bedrock erodes the bedrock profile and is a source of new sediment. No sediment deformation, basal sliding or bedrock erosion occurs when the base is below the ice pressure-melting point, when presumably there is insufficient liquid water to support most of the ice load and prevent sediment compaction.

In the marine experiments described below nothing happens to sediment in ice-free locations, except for an imposed maximum slope limit of 0.3° representing marine slumping down the continental slope, and an infinite sink of sediment to the deep ocean (i.e. no sediment allowed at the right hand edge of the figures below). There are no non-glacial sedimentary processes, and no pelagic deposition. Very similar ice-sediment models haves been applied to general Pleistocene cycles (Boulton, 1996) and Quaternary Barents-Sea deposits (Dowdeswell and Siegert, 1999; Howell and

Siegert, 2000). Other predictive ice sheet-sediment models have been developed by ten Brink and Schneider (1995), ten Brink *et al.* (1995), Tomkin and Braun (2002), Bougamont and Tulaczyk (2003), and Hildes *et al.* (2004).

BASIC RESULTS WITH CLIMATICALLY FORCED RETREATS

As preliminary tests of the model, 1-D flowline experiments have been run for 10 million years, with an initial linear equilibrium bedrock slope and constant sea level. Simple climatic patterns are prescribed for annual mean surface temperature T (°C) = –20 – 0.0051 × elevation (m), ice surface budget B (m yr^{-1}) = $0.15 \times 2^{(T+15)/10}$, and ocean shelf-melting M = 0.1 m yr^{-1}. These are constant except in experiments with forced ice retreats, in which a drastic decrease of B = –1 m yr^{-1} is imposed everywhere for 10^5 years once every 10^6 years causing complete wastage of all ice. As shown below, quite a wide variety of long-term ice and sediment behaviour occurs in the model depending on uncertain features such as sediment rheological parameters and initial bedrock geometry. The results are not intended to prove any particular conclusions, but just to illustrate the variety and uncertainty at this stage, and to suggest what may be possible in the future as more definitive models become available.

The most straightforward type of behaviour is shown in Fig. 1 using the nominal ice and sediment parameter values given in the Appendices. Ice sheet maximum extents do not vary much during the run, with the ice growing to nearly the same size after each forced retreat, limited to grounding line depths of <~500 m. Throughout the run fresh sediment is quarried by grounded ice acting on inland and inner-shelf bedrock, and quickly transported as deforming sediment to the grounding line where it accumulates in a wedge. This allows lengthy advances of grounded ice, as the sediment wedge reduces the bathymetry and grounding-line depths (Alley, 1991; Dahlgren *et al.*, 2002). After each forced retreat, a new wedge of sediment advances with the grounding line, resembling smaller-scale grounding-zone wedges of tidewater glaciers (Powell and Alley, 1997). The time scale of advance is on the order of 10^6 years (Fig. 1C), controlled not by ice mass balance but by grounding line-sediment interaction. When previous deposits are reached the new sediment is draped over them, first by piling up on the inner slope and then slumping down the steep outer slope, producing the laminated strata in Fig. 1B (discussed further below). A single large triangular deposit ~1000 m thick is formed after 10 million years.

SENSITIVITY EXPERIMENTS WITH CLIMATICALLY FORCED RETREATS

The simple structure of the sediment deposits in Fig. 1 is basically due to the small amount of total sediment transported to the shelf. There is not enough transport to cause very rapid slumping down the outer slopes of earlier deposits, or conversely to build large enough deposits that form barriers to later sediment wedges (both of which produce more complex patterns as seen below). One of the more uncertain variables in the sediment model is the viscosity μ_o, which can potentially affect total transport. Our nominal model value is 1×10^{10} Pa s, and we experimented with values between 1×10^9 and 1×10^{11}. This makes little difference to the results, and a single laminated triangular deposit is formed after 10 Ma much like Fig. 1 (not shown). [*n.b.* Although total sediment transport increases with decreasing μ_o at constant basal stress τ_b (Eq. B3), it *decreases* with decreasing μ_o at constant basal (sediment-top) velocity $u_s(0)$ (seen by combining (B2) and (B3)). When μ_o is changed in our interactive model, both basal stresses and velocities change as the ice sheet reacts to the different basal slipperiness, and the net effect on sediment transport is not readily deducible from the relations in Appendix B; in fact, it decreases slightly with decreasing μ_o, at least in the range 10^9 to 10^{11} Pa s.]

The basic properties of the sediment in this context are (i) sediment-top velocity $u_s(0)$ (affecting basal slipperiness and ice flow) and (ii) total sediment transport $\int u_s dz$ (affecting shelf accumulation), and their dependence on basal shear stress. If this combination can be changed outside the constraints of the weakly non-linear model, then very different long-term interactions between ice sheets and sediment deposits can ensue. Given current uncertainty in even the basic forms of sediment rheology, hydrology and transport mechanisms

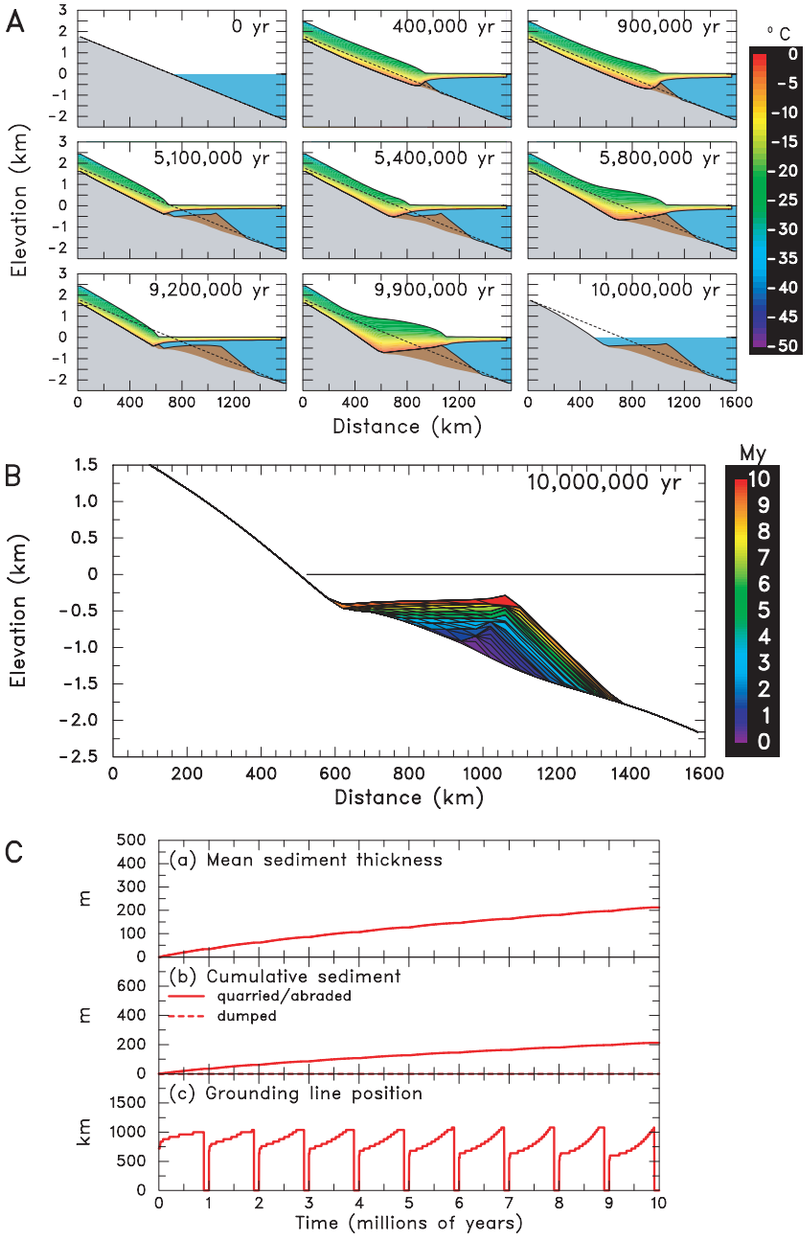

Fig. 1 Ten million year simulation with forced retreats every 1 million years, and with nominal ice and sediment model parameters. (**A**) Ice sheet temperatures (rainbow scale), bedrock (grey), sediment (brown) and ocean (blue), at various times through the run. (**B**) Isochrons of time of original sediment deposition at the end of the run. Times are relative to the start of the run. (**C**) Time series of (A) Sediment thickness averaged over the model domain; (B) Cumulative amounts of sediment sources and sinks averaged over the model domain, where 'dumped' refers to the deep-ocean sink at the right-hand boundary of the domain; (C) Grounding line position from the left-hand boundary of the domain.

under ice sheets, we suggest that this could be the case, due, for instance, to ploughing of plastic sediment by sub-ice bumps (Tulaczyk *et al.*, 2001). Instead of formulating completely different sediment models, here we explore different behaviours by crudely altering sediment model values within the weakly-non-linear framework. Specifically, we increase total sediment transport in Eq. (B3) by an *ad hoc* enhancement factor E. Further work with alternate rheologies and advection processes is needed to confirm that such modifications are reasonable, and to guide future choices in sub-ice sediment models.

Setting the sediment transport factor $E = 10$ produces quite different behaviour (Fig. 2). The sediments deposited in each advance (after the first three) form barriers to subsequent re-advances, so that new sediment wedges pile up in front of

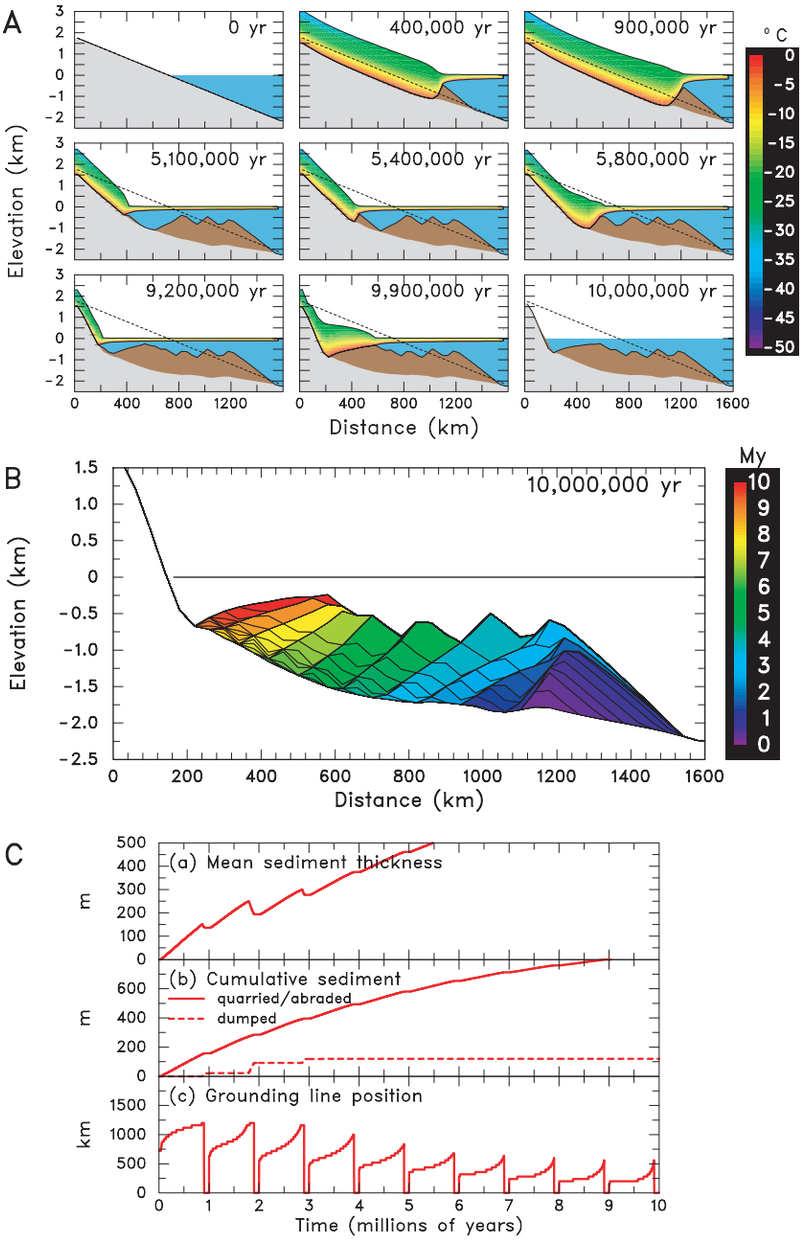

Fig. 2 10 million year simulation with forced retreats every 1 million years. As Fig. 1 except with sediment transport enhancement factor $E = 10$ (see text).

the earlier deposits but do not override them. As shown by the stratal patterns in Fig. 2B, a regular series of retrograding sediment units is formed, one per million years between the imposed retreats. The structure is arguably more realistic than the single laminated triangle in Fig. 1B, but still too regular.

More complex behaviour is shown in Fig. 3, with transport factor $E = 10$ *and* sediment viscosity μ_o reduced to 1×10^9 Pa s. The lower viscosity produces a more slippery bed, thinner ice and slightly less sediment transport than in Fig. 2. The first five re-advances (Fig. 3C) override the previous sediment, forming an early distal laminated wedge as in Fig. 1. The next readvance also overrides this wedge, and transports some of the earlier sediment to the top of the shelf break where it slumps to the deep ocean, forming an erosional

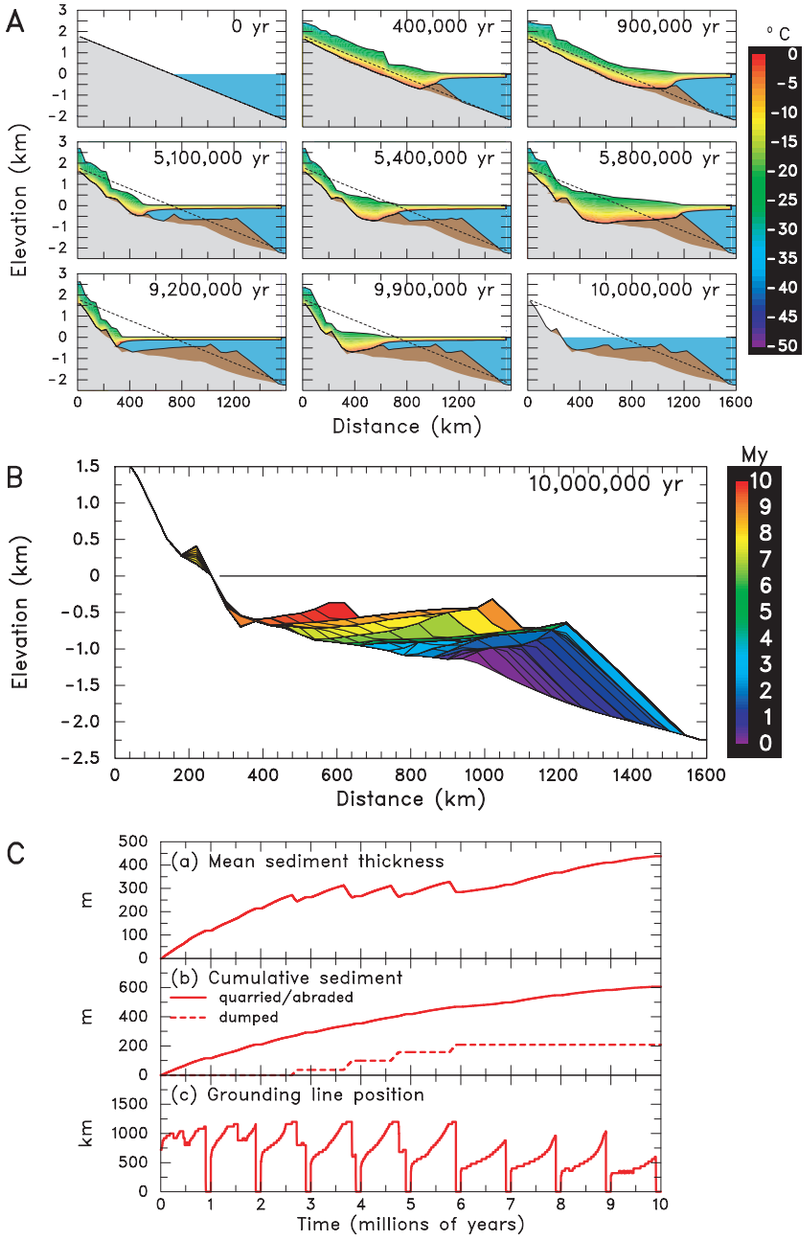

Fig. 3 10 million year simulation with forced retreats every 1 million years. As Fig. 1 except with sediment transport enhancement factor $E = 10$ and sediment viscosity decreased by $\times 0.1$ (to 1×10^9 Pa s).

unconformity at ~5–6 My. After 6 My, some readvances do not override the previous deposits, and an irregular retrograding sequence is formed on the inner shelf until the end of the run. By the last million years, bedrock erosion on the inner shelf (not replaced by sediment) has increased grounding line depths sufficiently to inhibit ice advance, and the last 'proximal' sediment wedge is deposited much closer to the land.

Another effect of the increased basal slipperiness in Fig. 3 is that grounded ice is thinner, especially on the steep inland bedrock slopes, so that basal temperatures are able to reach the freezing point in places. This allows sporadic higher frequency fluctuations due to the MacAyeal-Payne thermal mechanism (basal regions alternately freezing, inhibiting sliding, thickening, then warming and sliding again; MacAyeal, 1993). The resulting breaks

of ice surface slope are evident in Fig. 3A, and propagate downstream to the grounding line triggering minor retreats in the first 2 My of the run (Fig. 3C).

RESULTS WITH NO CLIMATIC VARIATIONS

If the prescribed climate is held constant (i.e. no temporal variations in the surface budget parameterization and no forced retreats, otherwise same as in Fig. 3), *unforced* internal oscillations of the ice-sediment-bedrock system occur, as shown in Fig. 4. They are mainly due to sudden groundin-line retreats triggered by the following mechanism (deduced from animations). When an advancing grounding-line sediment wedge reaches and overtops a topographic peak in the previous deposits (usually the outermost 'shelf break'), the maximum sediment slope of 0.3° is exceeded, and the wedge begins to slump down the pre-existing outer slope.

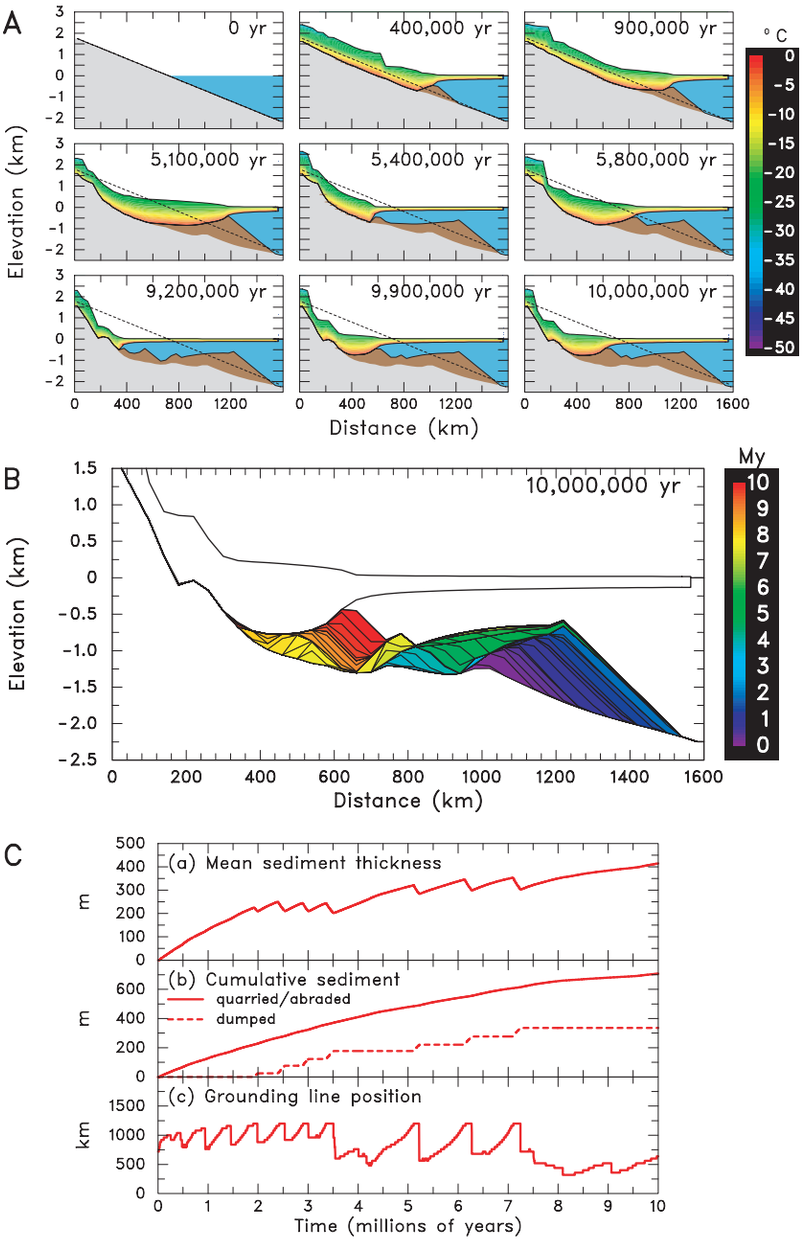

Fig. 4 10 million year simulation with constant climatic forcing, otherwise same as in Fig. 3.

The slumping exceeds the supply of deforming sediment transported under the ice, and the net loss of sediment causes a deepening of the grounding line (from ~500 to ~600 m), followed by rapid grounding-line retreat back down the inner slope of the peak. The largest such retreats occur at ~3.5, 5.2, 6.3 and 7.2 My in Fig 4C (panel (c)), and the associated slumping to the deep-ocean sink at the right-hand edge of the domain produces the steps in the 'dumped' curve in panel (b). This same mechanism also occurs just before some of the forced retreats in Fig. 3C.

Although all of the retreats in Fig. 4 are associated with the slumping mechanism, many of them are hastened or triggered by freeze-thaw fluctuations. As described above, higher-frequency basal freeze-thaw fluctuations propagate downstream to the grounding line and cause small transient variations in ice thickness there. Although these fluctuations are not required for the major retreats, they do induce many minor retreats that would not otherwise occur, especially in the first 3 My and after 8 My, and they affect the whole character of the time series in Fig. 4C. If the freeze-thaw switch is turned off (by allowing basal sliding and sediment deformation regardless of temperature), the resulting grounding-line time series is much more regular and smoothly oscillating (not shown).

COMPARISON OF MODEL STRATA WITH OBSERVATIONS

The panels in Figs. 1B–4B above show isochrons of the time of original sediment deposition, which represent 'strata' created by repeated cycles of deposition and erosion. They are plotted by tracking times of original deposition on an Eulerian grid with the same horizontal spacing as the model, and with fine (1-m) regular vertical spacing that shifts up and down with the bedrock (i.e. with $z = 0$ always at the bedrock-sediment interface). As the sediment-top surface moves upwards due to deposition (or downwards due to erosion) through a grid point, the value there is set to the current time (or is reset to null for no sediment). The resulting plots can be compared to observed strata and long-term history inferred from seismic profiles, in the spirit of ten Brink *et al.*'s (1995) studies.

One would not expect much agreement between these simple tests and Cenozoic Antarctic shelf deposits (such as generalized profiles in Cooper *et al.*, 1993). Nevertheless, the more complex stratal patterns in Figs. 3B and 4B do exhibit some features reminiscent of observed seismic profiles. During the first ~3 million years a prograding sequence of shelf breaks is produced in the distal sediments, as wedges are deposited in successive ice advances. This corresponds with prograding shelf breaks noted in the older sections of many seismic profiles by Barker (1995, his Fig. 8). There are some erosional unconformities in the middle parts of the runs, with later proximal sediment packages resting above them. The early-distal/late-proximal depositional sequences in the figures are suggestive of Barker's later aggrading/retrograding shelf breaks. Compared to the initial bedrock profile, there is a trend towards a reverse bathymetric slope with shallower depths on the outer shelf and greater depths on the inner shelf, as more inner-shelf bedrock is eroded and transported to the outer regions. This is a unique feature of continental shelves of glaciated land masses (Anderson, 1999) and has also been modelled by ten Brink and Schneider (1995) and ten Brink *et al.* (1995).

To emphasize the preliminary and unconstrained nature of these results, Fig. 5 shows the sediment isochron pattern for a very different 10 million year run with several model features not included above: a pre-existing continental shelf-like profile, prescribed pelagic sediment deposition, and imposed sea-level variations every 100 ka. The dominant sediment source is pelagic, and the earlier deposits are reworked considerably by sub-ice transport as the grounding line advances to the shelf edge. The resulting stratal pattern shows a pronounced unconformity overlain by the later (9 to 10 My) deposits, and bears little relationship to those above.

CONCLUDING REMARKS

The flowline model described here illustrates several potentially important long-term interactions between ice and sediment in the marine marginal environment. These include thinning and flattening of ice profiles by sediment deformation, shallowing of water depths by sediment accumulation on the continental shelf that allows

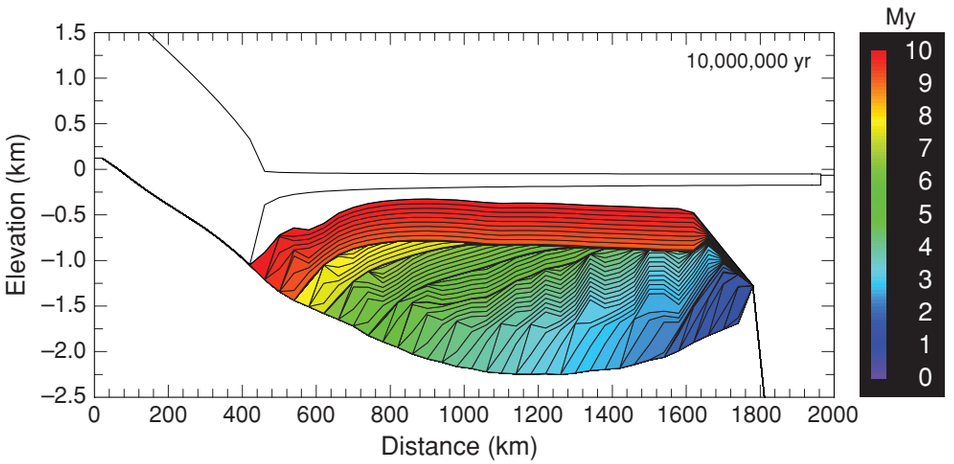

Fig. 5 Isochrons of time of original sediment deposition at the end of a 10 million year run with pre-existing shelf profile, pelagic deposition, 100 kyr sea-level variations, and modified sediment properties.

extensive grounding-line advances and retreats, initiation of drastic retreats by slumping of sediment wedges down pre-existing outer slopes, and stochastic effects of binge-purge fluctuations. A wide variety of sediment distributions and strata is produced on the continental shelf after 10 million years, with some features reminiscent of observed Antarctic margin profiles: notably the trend towards reverse bathymetric slope, and prograding shelf breaks on the outer shelf.

Although the wide variety of patterns produced by uncertain model parameter ranges precludes any definitive conclusions, it suggests what may be possible with more refined models in the future. One tentative conclusion from this study is that within the framework of the weakly non-linear sediment model (Appendix B), relatively featureless sediment distributions are produced (Fig. 1). The richer patterns in Figs. 2 to 5 require modifications that allow different combinations of sediment top velocity and total sediment transport as functions of basal stress, which may be indicative of very different basal sediment mechanisms and rheology (Tulaczyk *et al.*, 2001).

However, it is clear that none of the pictures above bears much overall resemblance to observed profiles, and serious comparisons with Antarctic shelf deposits would be premature. To link Cenozoic climate directly with Antarctic glacimarine deposits, progress will be needed in many modelling areas, including:

1 ascertaining climatic and oceanic forcing of the ice sheet through the Cenozoic on orbital to million year time scales;
2 including forcing factors of eustatic sea level and tectonics;
3 applying 2-D/3-D ice and sediment models to the geographies and histories of individual regions, taking into account geographic distributions of sedimentary sub-basins (De Santis *et al.*, 1999), terrestrial bed properties (Siegert *et al.*, 2005), and overall sediment inventories (Bougamont and Tulaczyk, 2003; Taylor *et al.*, 2004; Jamieson *et al.*, 2005); the single ~1000 km-long 'conveyor belt' for sediment in the flowline model above ignores any lateral sources or sinks;
4 constraining sediment rheologies and transport mechanisms (Tulaczyk *et al.*, 2001) and hydrology (MacAyeal, 1992; Breemer *et al.*, 2002; Flowers and Clarke, 2002);
5 including smaller-scale grounding-line wedge/bank processes (Powell and Alley, 1997).

ACKNOWLEDGEMENTS

We thank A. Hubbard and an anonymous reviewer for careful reviews that significantly helped the manuscript. This research was funded by the US National Science Foundation under awards ATM-0513402/0513421, ANT-0342484 and ANT-0424589.

REFERENCES

Alley, R.B. (1989) Water pressure coupling of sliding and bed deformation: II. Velocity-depth profiles. *J. Glaciol.*, **35**, 119–129.

Alley, R.B. (1991) Sedimentary processes may cause fluctuations of tidewater glaciers. *Ann. Glaciol.*, **15**, 119–124.

Alley, R.B. and Whillans, I.M. (1984) Response of the East Antarctic Ice Sheet to sea-level rise. *J. Geophys. Res.*, **89**, 6487–6493.

Anderson, J.B. (1999) *Antarctic Marine Geology*. Cambridge University Press, 289 pp.

Anderson, J.B. and Shipp, S.S. (2001) Evolution of the West Antarctic Ice Sheet. In: *The West Antarctic Ice Sheet: Behavior and Environment* (Eds R.B. Alley and R.A. Bindschadler), *Antarctic Research Series Vol. 77*, American Geophysical Union, Washington, D.C., 45–57.

Barker, P.F. (1995) The proximal marine sediment record of Antarctic climate since the late Miocene. In: *Geology and Seismic Stratigraphy of the Antarctic Margin* (Eds A.K. Cooper, P.F. Barker, G. Brancolini), *Antarctic Research Series Vol. 68*, American Geophysical Union, Washington D.C., 25–57.

Blatter, H. (1995) Velocity and stress fields in grounded glaciers: a simple algorithm for including deviatoric stress gradients. *J. Glaciol.*, **42**, 333–344.

Bougamont, M. and Tuylaczyk, S. (2003) Glacial erosion beneath ice streams and ice-stream tributaries: constraints on temporal and spatial distribution of erosion from numerical simulations of a West Antarctic ice stream. *Boreas*, **32**, 178–190.

Boulton, G.S. (1996) Theory of glacial erosion, transport and deposition as a consequence of subglacial sediment deformation. *J. Glaciol.*, **42**, 43–62.

Boulton, G.S. and Hindmarsh, R.C.A. (1987) Sediment deformation beneath glaciers: Rheology and geological consequences. *J. Geophys. Res.*, **92**, 9050–9082.

Brancolini, G., Cooper, A.K. and Coren, F. (1995) Seismic facies and glacial history in the western Ross Sea (Antarctica). In: *Geology and Seismic Stratigraphy of the Antarctic Margin* (Eds A.K. Cooper, P.F. Barker, G. Brancolini), *Antarctic Research Series Vol. 68*, American Geophysical Union, Washington D.C., 209–233.

Breemer, C.W., Clark, P.U. and Haggerty, R. (2002) Modeling the subglacial hydrology of the late Pleistocene Lake Michigan lobe, Laurentide ice sheet. *Geol. Soc. Am. Bull.*, **114**, 665–674.

Clark, P.U. and Pollard, D. (1998) Origin of the mid-Pleistocene transition by ice-sheet erosion of regolith. *Paleoceanography*, **13**, 1–9.

Cooper, A.K., Eittreim, S., ten Brink, U. and Zayatz, I. (1993) Cenozoic glacial sequences of the Antarctic continental margin as recorders of Antarctic ice sheet fluctuations. In: *The Antarctic Paleoenvironment: A Perspective on Global Change, Part Two* (Eds J.P. Kennett, D.A. Warnke), *Antarctic Research Series Vol. 60*, American Geophysical Union, Washington D.C., 75–89.

Dahlgren, K.I.T., Vorren, T.O. and Laberg, J.S. (2002) The role of grounding-line sediment supply in ice-sheet advances and growth on continental shelves: an example from the mid-Norwegian sector of the Fennoscandian ice sheet during the Saalian and Weichselian. *Quatern. Int.*, **95–96**, 25–33.

De Santis, L., Prato, S., Brancoloni, G., Lovo, M. and Torelli, L. (1999) The Eastern Ross Sea continental shelf during the Cenozoic: implications for the West Antarctic ice sheet development. *Global Planet. Change*, **23**, 173–196.

Dowdeswell, J.A. and Siegert, M.J. (1999) Ice-sheet numerical modeling and marine geophysical measurements of glacier-derived sedimentation on the Eurasian Arctic continental margins. *Geol. Soc. Am. Bull.*, **111**, 1080–1097.

Dupont, T.K. and Alley, R.B. (2005) Assessment of the importance of ice-shelf buttressing to ice-sheet flow. *Geophys. Res. Lett.*, **32**, L04503, doi: 10.1029/2004GL022024.

Escutia, C., De Santis, L., Donda, F., Dunbar, R.B., Cooper, A.K., Brancolini, G. and Eittreim, S.L. (2005) Cenozoic ice sheet history from East Antarctic Wilkes Land continental margin sediments. *Global Planet. Change*, **45**, 51–81.

Flowers, G.E. and Clarke, G.K.C. (2002) A multicomponent coupled model of glacier hydrology. 1. Theory and synthetic examples. *J. Geophys. Res.*, **107** (B11), 2287, doi: 10.1029/2001JB001122.

Hallet, B. (1996) Glacial quarrying: a simple theoretical model. *Ann. Glaciol.*, **22**, 1–8.

Hambrey, M.J. and Barrett, P.J. (1993) Cenozoic sedimentary and climatic record, Ross Sea region, Antarctica. In: *The Antarctic Paleoenvironment: A Perspective on Global Change, Part Two* (Eds J.P. Kennett, D.A. Warnke), *Antarctic Research Series Vol. 60*, American Geophysical Union, Washington D.C., 91–124.

Hildes, D.H.D., Clarke, G.K.C., Flowers, G.E. and Marshall, S.J. (2004) Subglacial erosion and englacial sediment transport modelled for North American ice sheets. *Quatern. Sci. Rev.*, **23**, 409–430.

Hindmarsh, R.C.A. (1993) Qualitative dynamics of marine ice sheets. In: I*ce in the Climate System*. (Ed. W.R. Peltier), *NATO Advanced Science Series I*: Global Environmental Change, vol. 12, Springer Verlag, Berlin, 67–99.

Hindmarsh, R.C.A. (1996) Stability of ice rises and uncoupled marine ice sheets. *Ann. Glaciol.*, **23**, 105–115.

Hindmarsh, R.C.A. (2004) A numerical comparison of approximations to the Stokes equations used in ice sheet and glacier modeling. *J. Geophys. Res.*, **109**, F01012, doi: 10.1029/2003JF000065, 1–15.

Hindmarsh, R.C.A. and LeMeur, E. (2001) Dynamical processes involved in the retreat of marine ice sheets. *J. Glaciol.*, **47**, 271–282.

Howell, D. and Siegert, M.J. (2000) Intercomparison of subglacial sediment-deformation models: application to the late Weichselian western Barents margin. *Ann Glaciol.*, **30**, 187–196.

Hubbard, A. (1999) High-resolution modeling of the advance of the Younger Dryas ice sheet and its climate in Scotland. *Quatern. Res.*, **52**, 27–43.

Hubbard, A. (2000) The verification and significance of three approaches to longitudinal stresses in high-resolution models of glacier flow. *Geogr. Ann.*, **62A**, 471–487.

Hubbard, A. (2006) The validation and sensitivity of a model of the Icelandic ice sheet. *Quatern. Sci. Rev.*, in press.

Hulbe, C.L. and MacAyeal, D.R. (1999) A new numerical model of coupled inland ice sheet, ice stream and ice shelf flow and its application to the West Antarctic ice sheet. *J. Geophys. Res.*, **104**, 25349–25366.

Huybrechts, P. (1990) A 3-D model for the Antarctic ice sheet: a sensitivity study on the glacial-interglacial contrast. *Clim. Dyn.*, **5**, 79–92.

Huybrechts, P. (1993) Glaciological modeling of the late Cenozoic East Antarctic ice sheet: stability or dynamism? *Geogr. Ann.*, **75A**, 221–238.

Huybrechts, P. (1994) Formation and disintegration of the Antarctic ice sheet. *Ann. Glaciol.*, **20**, 336–340.

Huybrechts, P. (1998) Report of the Third EISMINT Workshop on Model Intercomparison. European Science Foundation, Strasbourg, 105–120.

Huybrechts, P. (2002) Sea-level changes at the LGM from ice-dynamic reconstructions of the Greenland and Antarctic ice sheets during the glacial cycles. *Quatern. Sci. Rev.*, **21**, 203–231.

Jamieson, S.S.R., Hulton, N.R.J., Sugden, D.E., Payne, A.J. and Taylor, J. (2005) Cenozoic landscape evolution of the Lambert basin, East Antarctica: the relative role of rivers and ice sheets. *Global Planet. Change*, **45**, 35–49.

Jenson, J.W., MacAyeal, D.R., Clark, P.U., Ho, C.L. and Vela, J.C. (1996) Numerical modeling of subglacial sediment deformation: Implications for the behavior of the Lake Michigan lobe, Laurentide Ice Sheet. *J. Geophys. Res.*, **101**, B4, 8717–8728.

Kamb, B. (2001) Basal zone of the West Antarctic ice streams and its role in lubrication of their rapid motion. In: *The West Antarctic Ice Sheet: Behavior and Environment* (Eds R.B. Alley and R.A. Bindschadler), *Antarctic Research Series Vol. 77*, American Geophysical Union, Washington D.C., 157–199.

MacAyeal, D.R. (1989) Large-scale ice flow over a viscous basal sediment: theory and application to Ice Stream B, Antarctica. *J. Geophys. Res.*, **94**, B4, 4071–4087.

MacAyeal, D.R. (1992) Irregular oscillations of the West Antarctic ice sheet. *Nature*, **359**, 29–32.

MacAyeal, D.R. (1993) Binge-purge oscillations of the Laurentide ice sheet as a cause of the North Atlantic's Heinrich events. *Paleoceanography*, **8**, 775–784.

MacAyeal, D.R. (1996) EISMINT: Lessons in Ice-Sheet Modeling. Department of Geophysical Sciences, University of Chicago, 428 pp.

MacAyeal, D.R. and Thomas, R.H. (1982) Numerical modeling of ice shelf motion. *Ann. Glaciol.*, **3**, 189–193.

Maqueda, M.A.M., Willmott, A.J., Bamber, J.L. and Darby, M.S. (1998) An investigation of the Small Ice Cap Instability in the Southern Hemisphere with a coupled atmosphere-sea ice-ocean terrestrial ice model. *Clim. Dyn.*, **14**, 329–352.

Marshall, S.J. and Clarke, G.K.C. (1997) A continuum mixture of ice stream thermodynamics in the Laurentide Ice Sheet. 1. Theory. *J. Geophys. Res.*, **102**, B9, 20599–20613.

Marshall, S.J., Bjornsson, H., Flowers, G.E. and Clarke, G.K.C. (2005) Simulation of Vatnajokull ice cap dynamics. *J. Geophys. Res.*, **110**, F03009, doi: 10.1029/2004JF000262.

Miller, M.F. and Mabin, M.C.G. (1998) Antarctic Neogene landscapes – in the refrigerator or in the deep freeze? *GSA Today*, Geol. Soc. Amer., **8**(4), 1–8.

Morland, L.W. (1987) Unconfined ice-shelf flow. In: *Dynamics of the West Antarctic Ice Sheet* (Eds C.J. van der Veen and J. Oerlemans), Springer, New York, 99–116.

Oerlemans, J. (2002) On glacial inception and orography. *Quatern. Int.*, **95–96**, 5–10.

Oerlemans, J. (2004a) Correcting the Cenozoic $\delta^{18}O$ deep-sea temperature record for Antarctic ice volume. *Palaeogeogr. Palaeoclimatol. Palaeoecol.*, **208**, 195–205.

Oerlemans, J. (2004b) Antarctic ice volume and deep-sea temperature during the last 50 Ma: a model study. *Ann. Glaciol.*, **39**, 13–19.

Pagani, M., Zachos, J.C., Freeman, K.H., Tipple, B. and Bohaty, S. (2005) Marked decline in atmospheric carbon dioxide concentrations during the Paleogene. *Science*, **309**, 600–603.

Pattyn, F. (2002) Transient glacier response with a higher-order numerical ice-flow model. *J. Glaciol.*, **48**, 467–477.

Pattyn, F. (2003) A new three-dimensional higher-order thermomechanical ice sheet model: Basic sensitivity, ice stream development, and ice flow across subglacial lakes. *J. Geophys. Res.*, **108**, B8, 2382, doi: 10.1029/2002JB002329.

Payne, A.J., Vieli, A., Shepherd, A.P., Wingham, D.J. and Rignot, E. (2004) Recent dramatic thinning pf largest West Antarctic ice stream triggered by oceans. *Geophys. Res. Lett.*, **31**, L23401, doi: 10.1029/2004GL021284, 1–4.

Pekar, S.F. and DeConto, R. (2006) High-resolution ice-volume estimates for the early Miocene: Evidence for a dynamic ice sheet in Antarctica. *Palaeogeogr. Palaeoclimatol. Palaeoecol.*, **231**, 101–109.

Pekar, S.F., Harwood, D. and DeConto, R. (2006) Resolving a late Oligocene conundrum: deep-sea warming versus Antarctic glaciation. *Palaeogeogr. Palaeoclimatol. Palaeoecol.*, **231**, 29–40.

Pollard, D. and DeConto, R.M. (2003) Antarctic ice and sediment flux in the Oligocene simulated by a climate-ice sheet-sediment model. *Palaeogeogr. Palaeoclimatol. Palaeoecol.*, **198**, 53–67.

Powell, R.D. and Alley, R.B. (1997) Grounding-line systems: processes, glaciological inferences and the stratigraphic record. In: *Geology and Seismic Stratigraphy of the Antarctic Margin, Part 2* (Eds P.F. Barker and A.K. Cooper), *Antarctic Research Series Vol. 71*, American Geophysical Union, Washington D.C., 169–187.

Ritz, C., Fabre, A. and Letreguilly, A. (1997) Sensitivity of a Greenland ice sheet model to ice flow and ablation parameters: consequences for the evolution through the last climatic cycle. *Clim. Dyn.*, **13**, 11–24.

Ritz, C., Rommelaere, V. and Dumas, C. (2001) Modeling the evolution of Antarctic ice sheet over the last 420,000 years: Implications for altitude changes in the Vostok region. *J. Geophys., Res.*, **106**, D23, 31943–31964.

Scherer, R.P. (1991) Quaternary and Tertiary microfossils from beneath Ice Stream B – evidence for a dynamic West Antarctic Ice Sheet history. *Global Planet. Change*, **90**, 395–412.

Siegert, M.J., Taylor, J. and Payne, A.J. (2005) Spectral roughness of subglacial topography and implications for former ice-sheet dynamics in East Antarctica. *Global Planet. Change*, **45**, 249–263.

Taylor, J., Siegert, M.J., Payne, A.J., Hambrey, M.J., O'Brien, P.E., Cooper, A.K. and Leitchenkov G. (2004) Topographic controls on post-Oligocene changes in ice-sheet dynamics, Prydz Bay region, East Antarctica. *Geology*, **32**, 197–200.

ten Brink, U.S. and Schneider, C. (1995) Glacial morphology and depositional sequences of the Antarctic continental shelf. *Geology*, **23**, 580–584.

ten Brink, U.S., Schneider, C. and Johnson, A.H. (1995) Morphology and stratal geometry of the Antarctic continental shelf: insights from models. In: *Geology and Seismic Stratigraphy of the Antarctic Margin* (Eds A.K. Cooper, P.F. Barker, G. Brancolini), *Antarctic Research Series Vol. 68*, American Geophysical Union, Washington D.C., 1–24.

Tomkin, J.H. and Braun, J. (2002) The influence of Alpine glaciation on the relief of tectonically active mountain belts. *Am. J. Sci.*, **302**, 169–190.

Tulaczyk, S., Kamb, W.B. and Engelhardt, H.F. (2000) Basal mechanics of Ice Stream B, West Antarctica 1. Till mechanics. *J. Geophys. Res.*, **105**, B1, 463–481.

Tulaczyk, S.M., Scherer, R.P. and Clark, C.D. (2001) A ploughing model for the origin of weak tills beneath ice streams: a qualitative treatment. *Quatern. Int.*, **86**, 59–70.

van der Veen, C.J. (1985) Response of a marine ice sheet to changes at the grounding line. *Quatern. Res.*, **24**, 257–267.

Vieli, A. and Payne, A.J. (2005) Assessing the ability of numerical ice sheet models to simulate grounding line migration. *J. Geophys. Res.*, **110**, F01003, doi: 10.1029/2004JF000202, 1–18.

Weertman, J. (1974) Stability of the junction of an ice sheet and an ice shelf. *J. Glaciol.*, **13**, 3–11.

Zachos, J., Pagani, M., Sloan, L. and Thomas, E. (2001) Trends, rhythms, and aberrations in global climate 65 Ma to present. *Science*, **292**, 686–693.

APPENDIX A

COMBINED ICE SHEET-SHELF EQUATIONS

The ice flow equations are solved for ice velocities, given the current state of the ice (ice thickness, temperatures, bed topography, basal properties and sea level). As outlined above, we use a heuristic combination of two standard sets of scaled equations, individually called 'shear' (for internal shear $\partial u/\partial z$) and 'stretching' (for vertical-mean longitudinal $\partial u/\partial x$). They are combined by including shear-softening terms due to each type of flow in the other's equations, and more importantly, by (i) using average horizontal velocity $\bar{u} = \bar{u}_i + u_b$ in the stretching equation, where $\bar{u}_i$ is the vertical mean of the internal shear flow and u_b is the basal velocity, (ii) including basal stress dependent on u_b in the stretching equation, and (iii) reducing the driving stress in the shear equations by the gradient of the longitudinal stress from the stretching equations acting on the column above each level.

Symbols are listed in Table A1. Two horizontal dimensions are included, although the paper reports only on 1-D flowline applications. 'Coupling' terms that are not usually found in purely sheet or purely

Table A1 Ice-flow notation and nominal values

x,y	Orthogonal horizontal coordinates (m)
z	Vertical coordinate, increasing upwards from a flat reference plane (m)
z_b	Elevation of ice base (m)
u, u_i, u_b	Horizontal ice velocities in x direction. u = total, u_i = internal deformation, u_b = basal (m yr^{-1})
v, v_i, v_b	Horizontal ice velocities in y direction. v = total, v_i = internal deformation, v_b = basal (m yr^{-1})
H	Ice thickness (m)
h	Ice surface elevation (m)
h_b	Ice base (bedrock or sediment top) elevation (m)
S	Sea level (m)
ρ	Ice density (910 kg m^{-3})
ρ_w	Water density (1000 kg m^{-3})
g	Gravitational acceleration (9.80616 m s^{-2})
A	Ice rheological coefficient (1×10^{-17} yr^{-1} Pa^{-3} at melt point, with temperature dependence as in Ritz *et al.*, 1997, 2001)
n	Ice rheological exponent (3)
B	Basal sliding coefficient between bedrock and ice (0.5×10^{-11} m yr^{-1} Pa^{-2} at melt point, ramping to 0 at −10°C)
m	Basal sliding exponent (2)
k	Floating versus basal sliding flag (0 or 1)
$\dot{\varepsilon}_{ij}$	Strain rate components (yr^{-1})
$\dot{\varepsilon}$	Effective strain rate, 2nd invariant (yr^{-1})
σ_{ij}	Deviatoric stress components (Pa)
σ	Effective stress, 2nd invariant (Pa)
μ	$^1/_2\ \dot{\varepsilon}^{(1-n)/n}$ (yr$^{2/3}$)
LHS_x, LHS_y	Left-hand sides of Eqs. 2a, 2b (Pa)

shelf formulations are identified by a dashed box. Writing Cartesian horizontal ice velocities as $u(x,y,z)$ and $v(x,y,z)$, define the basal ice velocity $u_b(x,y) = u(x,y,z_b)$, and the internal shearing ice velocity $u_i(x,y,z) = u - u_b$, so that $u_i(x,y,z_b) = 0$. Denoting vertical averages through the ice column by an overbar, then $\bar{u} = u_b + \bar{u}_i$ (and similarly for v_b, v_i and $\bar{v}$). The internal shear equations for $u_i(x,y,z)$ and $v_i(x,y,z)$ are

$$\frac{\partial u_i}{\partial z} = 2A\left[\sigma_{xz}^2 + \sigma_{yz}^2 + \boxed{\sigma_{xx}^2 + \sigma_{yy}^2 + \sigma_{xy}^2 + \sigma_{xx}\sigma_{yy}}\right]^{\frac{n-1}{2}}\sigma_{xz} \tag{A1a}$$

$$\frac{\partial v_i}{\partial z} = 2A\left[\sigma_{xz}^2 + \sigma_{yz}^2 + \boxed{\sigma_{xx}^2 + \sigma_{yy}^2 + \sigma_{xy}^2 + \sigma_{xx}\sigma_{yy}}\right]^{\frac{n-1}{2}}\sigma_{yz} \tag{A1b}$$

and the horizontal stretching equations for $\bar{u}$(x, y) and $\bar{v}$(x, y) are

$$\frac{\partial}{\partial x}\left[\frac{2\mu H}{\bar{A}^{1/n}}\left(2\frac{\partial \bar{u}}{\partial x} + \frac{\partial \bar{v}}{\partial y}\right)\right] + \frac{\partial}{\partial y}\left[\frac{\mu H}{\bar{A}^{1/n}}\left(2\frac{\partial \bar{u}}{\partial y} + \frac{\partial \bar{v}}{\partial x}\right)\right]$$
$$= \rho g H \frac{\partial h}{\partial x} + \boxed{\frac{k}{B^{1/m}}\left|u_b^2 + v_b^2\right|^{\frac{1-m}{2m}} u_b} \tag{A2a}$$

$$\frac{\partial}{\partial y}\left[\frac{2\mu H}{\bar{A}^{1/n}}\left(2\frac{\partial \bar{v}}{\partial y} + \frac{\partial \bar{u}}{\partial x}\right)\right] + \frac{\partial}{\partial x}\left[\frac{\mu H}{\bar{A}^{1/n}}\left(2\frac{\partial \bar{u}}{\partial y} + \frac{\partial \bar{v}}{\partial x}\right)\right]$$
$$= \rho g H \frac{\partial h}{\partial y} + \boxed{\frac{k}{B^{1/m}}\left|u_b^2 + v_b^2\right|^{\frac{1-m}{2m}} v_b} \tag{A2a}$$

Equations (A2a,b) and their horizontal boundary conditions for unconfined ice shelves are derived for instance in Morland (1982) and MacAyeal (1996). In the zero-order shallow ice approximation, the vertical shear stress (σ_{xz}, σ_{yz}) in Eqs. (A1a,b) would be balanced only by the hydrostatic driving force $-\rho g(h - z)(\partial h/\partial x, \partial h/\partial y)$ acting on the ice column above level z. Here, horizontal stretching forces are included in this force balance (Hubbard, 1999, 2006; Marshall *et al.*, 2005), so that

$$\sigma_{xz} = -\left(\rho g H \frac{\partial h}{\partial x} - \boxed{LHS_x}\right)\left(\frac{h - z}{H}\right),$$
$$\sigma_{yz} = -\left(\rho g H \frac{\partial h}{\partial y} - \boxed{LHS_y}\right)\left(\frac{h - z}{H}\right), \tag{A3}$$

where LHS_x and LHS_y are the left-hand sides of (A2a) and (A2b) respectively. Because horizontal stretching forces are taken to be vertically uniform and the terms in (A2) are forces on the whole ice thickness, their effect on the ice column above level z is scaled by $(h - z)/H$ in (A3).

Inclusion of the strain softening terms in (A1) and (A2) due to each other's flow requires manipulation of the constitutive relation for ice rheology. In (A2a,b),

$$\mu = \frac{1}{2}(\dot{\varepsilon}^2)^{\frac{1-n}{2n}} \tag{A4}$$

and $\bar{A} = \frac{1}{H}\int A dz$ is the vertical mean of the Arrhenius temperature-dependent coefficient in the constitutive relation

$$\dot{\varepsilon}_{ij} = A(T)(\sigma^2)^{\frac{n-1}{2}}\sigma_{ij} \quad \text{or}$$

equivalently $\dot{\varepsilon}_{ij} = (A(T))^{\frac{1}{n}}(\dot{\varepsilon}^2)^{\frac{n-1}{2n}}\sigma_{ij}$,

where $\dot{\varepsilon}_{ij}$ are strain rates, σ_{ij} are deviatoric stresses, and $\dot{\varepsilon}$ and σ are the second invariants of their respective tensors. The latter are defined by $\dot{\varepsilon}^2 \equiv \sum_{ij}\frac{1}{2}\dot{\varepsilon}_{ij}\dot{\varepsilon}_{ij}$ and $\sigma^2 \equiv \sum_{ij}\frac{1}{2}\sigma_{ij}\sigma_{ij}$. The relationship

$$\dot{\varepsilon}^2 \approx \left(\frac{\partial \bar{u}}{\partial x}\right)^2 + \left(\frac{\partial \bar{v}}{\partial y}\right)^2 + \frac{\partial \bar{u}}{\partial x}\frac{\partial \bar{v}}{\partial y} + \frac{1}{4}\left(\frac{\partial \bar{u}}{\partial y} + \frac{\partial \bar{v}}{\partial x}\right)^2 + \boxed{\frac{1}{4}\left(\frac{\overline{\partial u_i}}{\partial z}\right)^2 + \frac{1}{4}\left(\frac{\overline{\partial v_i}}{\partial z}\right)^2} \tag{A5}$$

is used to set μ in (A2a,b), and follows using

$$\dot{\varepsilon}^2 = \dot{\varepsilon}_{xx}^2 + \dot{\varepsilon}_{yy}^2 + \dot{\varepsilon}_{xx}\dot{\varepsilon}_{yy} + \dot{\varepsilon}_{xy}^2 + \dot{\varepsilon}_{xz}^2 + \dot{\varepsilon}_{yz}^2,$$

$$\dot{\varepsilon}_{xx} + \dot{\varepsilon}_{yy} + \dot{\varepsilon}_{zz} = 0, \quad \text{and}$$

$$\dot{\varepsilon}_{xx} = \frac{\partial \bar{u}}{\partial x},\ \dot{\varepsilon}_{yy} = \frac{\partial \bar{v}}{\partial y},\ \dot{\varepsilon}_{xy} = \frac{1}{2}\left(\frac{\partial \bar{u}}{\partial y} + \frac{\partial \bar{v}}{\partial x}\right),$$

$$\dot{\varepsilon}_{xz} \approx \frac{1}{2}\frac{\overline{\partial u_i}}{\partial z},\ \dot{\varepsilon}_{yz} \approx \frac{1}{2}\frac{\overline{\partial v_i}}{\partial z}.$$

The corresponding expression for σ^2 is used in (A1a,b), and the purely horizontal components are obtained in our numerical procedure from

$$\boxed{\sigma_{xx}^2 + \sigma_{yy}^2 + \sigma_{xy}^2 + \sigma_{xx}\sigma_{yy} = \left(\frac{2\mu}{\bar{A}^{1/n}}\right)^2\left[\left(\frac{\partial \bar{u}}{\partial x}\right)^2 + \left(\frac{\partial \bar{v}}{\partial y}\right)^2 + \frac{\partial \bar{u}}{\partial x}\frac{\partial \bar{v}}{\partial y} + \frac{1}{4}\left(\frac{\partial \bar{u}}{\partial x} + \frac{\partial \bar{v}}{\partial y}\right)^2\right]} \tag{A6}$$

The basal sliding relation used on the right-hand sides of (A2a) and (A2b) for grounded ice is $\tilde{u}_b = B|\tau_b|^{m-1}\tilde{\tau}_b$, or equivalently $\tilde{\tau}_b = B^{-\frac{1}{m}}|u_b|^{\frac{1-m}{m}}\tilde{u}_b$. Where ice is grounded, i.e. where $\rho_w(S - h_b) < \rho H$ or the ocean has no access (held back by intervening thicker ice or higher land), then $k = 1$ in the sliding terms, and the ice surface elevation $h = H + h_b$. Where ice is floating, i.e. $\rho_w(S - h_b) > \rho H$ and the ocean has access, then $k = 0$ and $h = S + H\,(1 - \rho/\rho_w)$.

At each timestep an iteration is performed between the two sets of equations (A1a,b) and (A2a,b). First, the elliptical system (A2) is solved for $\bar{u}$ and $\bar{v}$ by a sparse matrix algorithm, using the previous iteration's $\bar{u}_i$ and $\bar{v}_i$ where needed (to obtain μ via (A4) and (A5), and to relate u_b and v_b to $\bar{u}$ and $\bar{v}$). A standard sub-iteration is used in this step to account for the non-linear dependence of viscosity μ on $\bar{u}$ and $\bar{v}$ in (A4–5). Then (A1a,b) are solved to obtain the internal deformation flow $u_i(z)$ and $v_i(z)$ for each ice column, using LHS_x and LHS_y from the previous solution of (A2) to modify the driving stresses $\rho g H \partial h/\partial x$ and $\rho g H \partial h/\partial y$ in (A3), and using horizontal gradients of the previous $\bar{u}$ and $\bar{v}$ for the strain-softening terms in (A6). This iteration converges naturally to the appropriate scaling depending on the magnitude of the basal drag coefficient. Usually the flow is either almost all internal shear and basal drag balancing the driving stress, with negligible stretching, or is almost all longitudinal stretching balancing the driving stress, with small or no basal drag and negligible internal shear. For a narrow range of small basal drag coefficients, significant amounts of both flow types co-exist. The combination is heuristic because neither set of equations is accurate in the transition region where both $\partial u/\partial x$ and $\partial u/\partial z$ are non-negligible.

APPENDIX B

SEDIMENT MODEL EQUATIONS

The model of sediment deformation under ice follows Jenson *et al.* (1996), assuming a weakly non-linear till rheology (Boulton and Hindmarsh, 1987; Alley, 1989; Boulton, 1996). The same basic model has been applied to North American sediment distributions in the Quaternary (Clark and Pollard, 1998) and to Cenozoic Antarctic terrestrial sediments (Pollard and DeConto, 2003). When basal temperatures are at the ice pressure-melting point, the sediment is assumed saturated, and the effective stress (ice load minus water pressure) is assumed

Table B1 Sediment model notation and nominal values

z	Vertical coordinate, increasing downwards (m)
z_d	Depth below which $u_s = 0$ (m)
u_s	Horizontal sediment velocity (m s^{-1})
h_s	Sediment thickness (m)
f_b	Fractional area of exposed bedrock (0 to 1)
τ_b	Basal ice shear stress (Pa)
μ_0	Newtonian reference sediment viscosity (1×10^{10} Pa s)
D_0	Newtonian reference deformation rate (7.9×10^{-7} s^{-1})
p	Sediment rheologic exponent (1.25)
c	Sediment cohesion (0 Pa)
ϕ	Sediment angle of internal friction (22°)
E	Sediment transport enhancement factor (1)
S_{erode}	Quarrying or abrasion rate of exposed bedrock (m s^{-1})
ρ_s	Sediment density (2390 kg m^{-3})
ρ_b	Bedrock density (3370 kg m^{-3})
ρ_w	Liquid water density (1000 kg m^{-3})
g	Gravitational acceleration (9.80616 m s^{-2})

to be essentially zero at the ice-sediment interface and increases downward due to the buoyant weight of the sediment. The basal shear stress τ_b applied by the ice is assumed to be constant with depth in the sediment. Under these conditions the sediment stress-strain relationship is (Jenson *et al.*, 1996):

$$\tau_b = c + (\rho_s - \rho_w) g z \tan\phi + (2D_0)^{\frac{p-1}{p}} \mu_0 \left(-\frac{\partial u_s}{\partial z} \right)^{\frac{1}{p}} \quad \text{(B1)}$$

where z increases downwards from 0 at the ice-sediment interface (see Table B1). As discussed below, the sediment is assumed deep enough to always accomodate the deforming profile, so the bottom sediment-bedrock boundary has no effect. Neglecting sediment cohesion ($c = 0$), Eq. (B1) is integrated between the ice-sediment interface ($z = 0$) and the depth below which u_s is zero [$z_d = \tau_b / (\rho_s - \rho_w)\, g \tan\phi$], yielding the sediment top velocity

$$u_s(0) = \frac{\tau_b^{p+1}}{(\rho + 1)(\rho_s - \rho_w)\, g \tan\phi\, (2D_0)^{p-1} \mu_0^p} \quad \text{(B2)}$$

This velocity is imparted to the ice and produces additional ice transport in the ice-sheet advection equation (and is equal to u_b in the ice flow model assuming no sliding at the sediment–ice interface). The total horizontal transport of sediment over the deforming column is

$$\int_0^{z_d} u_s dz = \frac{E \tau_b^{p+2}}{(\rho + 2)(\rho + 1)[(\rho_s - \rho_w)\, g \tan\phi]^2 (2D_0)^{p-1} \mu_0^p} \quad \text{(B3)}$$

E is an *ad hoc* transport enhancement factor (see text). This expression is used for sediment transport in the sediment mass continuity equation

$$\frac{\partial h_s}{\partial t} = -\frac{\partial}{\partial x} \left[(1 - f_b) \int_0^{z_d} u_s dz \right] + f_b \frac{\rho_b}{\rho_s} S_{erode} \quad \text{(B4)}$$

where S_{erode} is the local rate of quarrying or abrasion by basal ice acting on exposed bedrock (Hallet, 1996). It is taken to be proportional to the work done by basal stress, i.e. $S_{erode} = 0.6 \times 10^{-9}\ \tau_b\, u_b$ where the units of τ_b are Pascals. For grid-mean sediment thicknesses h_s less than 0.5 m, the fractional area of exposed bedrock f_b is parameterized as $1 - (h_s / 0.5)$, and the patches of sediment are assumed to remain deep enough to accomodate the deforming profile (i.e. deeper than z_d). The basal ice velocity u_b ($= u_s(0)$) is assumed to be uniform within a grid cell, and separate basal shear stresses are calculated over sediment and exposed bedrock patches, which are weighted by $1 - f_b$ and f_b respectively to obtain the grid-mean τ_b. For $h_s \geq 0.5$ m, $f_b = 0$.

No sediment deformation, basal sliding or bedrock erosion occurs when the base is below the ice pressure-melting point, when presumably there is insufficient liquid water to support most of the ice load and prevent sediment compaction. For the marine applications of this paper, a maximum slope limit of 0.3° is imposed for submerged ice-free sediment surfaces, crudely representing slumping down the continental slope. Also, any sediment transported or slumped to the right-hand boundary of the domain is immediately removed, representing an infinite sink of sediment to the continental rise.